Printed ISSN 1330–0016
Online ISSN 1333–9133
CD ISSN 1333–8390
CODEN FIZBE7

CONTINUUM STATES IN NEUTRON-RICH CALCIUM AND NICKEL NUCLEI

M. BHATTACHARYA and G. GANGOPADHYAY

Department of Physics, University of Calcutta, 92, Acharya Prafulla Chandra Road, Kolkata-700 009, India

Received 16 October 2006; Revised manuscript received 26 December 2007
Accepted 28 December 2007 Online 15 February 2008

The effect of the resonant continuum on Ca and Ni nuclei near the neutron drip line has been investigated. The relativistic mean-field equations are solved using scattering-like conditions for the positive energy states. Pairing is implemented through a zero range interaction and the BCS equations are solved including the resonant states. We find that our calculation can reproduce the values for binding energy, radius, two-neutron separation energy, etc. in most cases. The nuclei ^{70,72}Ca show a sudden increase in the tail of the density distribution as the $3s_{1/2}$ state, being very weakly bound and having no centrifugal barrier, extends outside the nucleus radius to a large distance creating a neutron halo. Ni isotopes do not show any neutron halo. Appearance of new magic number and disappearance of the old ones in neutron-rich isotopes lead to dramatic difference in the drip line for even- and odd-mass nuclei in the two chains.

PACS numbers: 21.60.Jz,27.40.+z,27.50.+e,27.60.+j UDC 539.142, 539.144, 539.17

Keywords: Ca and Ni nuclei, neutron rich isotopes, resonant continua, relativistic mean-field equations, binding energy, radius, two-neutron separation energy, neutron halo, new magic number

1. Introduction

A large number of recent studies in nuclear structure has been devoted to nuclei with large neutron excesses. Experiments using radioactive ion beams and fission fragment studies have made it possible to produce and study a number of such nuclei. They exhibit various features distinctly different from their counterparts near the stability valley. Major surprises in the structure of nuclei very close to the neutron drip line include neutron skin and halo, quenching of spin-orbit splitting, the disappearance of the normal shell closures observed near the stability valley along with the emergence of new magic numbers, etc. [1]. The last bound neutrons

in such a nucleus lie very close to the continuum. The effect of the positive energy continuum on the structure of such nuclei should be studied carefully. Pairing interaction is also expected to play an important role in stabilizing the even-even nuclei.

One of the major tools of nuclear structure study is the mean-field approach. The usual practice of solving the mean-field equations is to expand them in a suitable basis, very often the harmonic oscillator basis. However, it is obvious that expansion in harmonic oscillator basis cannot explain the density of halo nuclei near the drip line because of slow convergence in the asymptotic region. Hartree-Fock-Bogoliubov (HFB) and relativistic Hartree-Bogoliubov (RHB) methods in coordinate space have emerged as two very accurate approaches of treating the nuclei very close to the drip line. The effect of the states in the continuum has been incorporated in most of these calculations by solving the equations in coordinate space using the box normalization condition, thus replacing the continuum with a set of discrete positive energy states. In nuclei near the stability valley, this procedure works well, because the contributions of continuum states are small far away from the Fermi level. However, in neutron rich nuclei near the drip line, the Fermi level is very close to the continuum and the positive energy states are expected to affect the results significantly. In this situation, the application of the box normalization procedure is open to question. Besides, in this procedure, the single-particle energy levels depend on the size of the box chosen, introducing an unwelcome feature.

Nonrelativistic Hartree-Fock equations involving continuum states have been solved with exact boundary conditions [2, 3] for zero-range and finite-range pairing forces. Relativistic mean field (RMF) equations involving continuum states have also been solved [4, 5] with exact boundary conditions. All these calculations have also taken into account the width of the continuum levels. For example, Cao and Ma [5] have also compared their results with those from calculations with zero width. They conclude that the pairing gaps, the Fermi energy, the pairing correlation energies and binding energies are considerably affected by proper consideration of the width of the resonant states. Particularly, near the neutron drip line, this effect is expected to be very important.

In the present work, we study the effect of the continuum states on the structure of Ca and Ni isotopes in the relativistic mean-field formalism, particularly in the vicinity of the neutron drip line. There have been numerous calculations on neutron rich Ca and Ni isotopes up to the neutron drip line using relativistic and nonrelativistic mean-field approaches. We list only a few that have been published recently. Nonrelativistic Hartree-Fock (HF) and Hartree-Fock-Bogoliubov approaches have been used by Fayans et al. [6] and Im and Meng [7]. Relativistic density-dependent Hartree-Fock approach [8] as well as relativistic-continuum Hartree-Bogoliubov method (RCHB) [9] have also been utilized to study neutron rich Ca isotopes [10, 11]. Meng et al. [12] have also used this method to study exotic systems from very light to very heavy mass including Ca and Ni nuclei. Yadav et al. [13] have performed RMF + BCS calculation on Ca and Ni isotopes by discretizing the continuum with box normalization. The problem of asymptotic behaviour at large radius has been overcome using expansion in a Woods-Saxon basis in a RMF

calculation [14]. Terasaki et al. [15] have studied even-even Ni isotopes between the proton and the neutron drip lines using HFB approach in three dimensions. Cao and Ma [5] have studied neutron-rich even Ni isotopes taking into account the resonance states in the continuum. Grasso et al. [16] have also studied the nuclei near the neutron drip line in Ca, Ni and Zr isotopes for giant neutron halos in the nonrelativistic mean field approach and compared different effective interactions. An alternative treatment for treating the resonant single-particle states is the analytic continuation of coupling constant method used by Zhang et al. [17]. In an earlier work, we have studied different properties like binding energy, single particle structure and radius in very neutron rich Ca and Ni nuclei and investigated the location of the drip line in even and odd isotopes [18]. The continuum RMF approach has not yet been utilized to study even Ca isotopes in detail. Even Ni isotopes have been studied [5] using constant pairing interaction only.

The aim of the present work is to investigate in detail the chains of Ca and Ni nuclei up to the neutron drip line using a zero-range interaction. The resonance states in the continuum have been explicitly included in the calculation. We aim to study the role of the resonant states near the drip line. We will see that the RMF theory with coupling to the continuum states can give a description comparable to the more elaborate RCHB calculation.

2. Results

The relativistic mean-field theory is very well known. Readers are referred to Refs. [19] – [22] for details regarding the theory and to Ref. [4] for the equations involving the resonant continuum. We have used the blocking approximation for odd-mass nuclei. The pairing calculation is done for the even neutron number less by one from the actual odd number and taking into account the state the last odd nucleon will occupy. After the convergence is achieved in the pairing calculation, the last odd neutron is placed in the desired state and the densities and energies are calculated. Thus we have calculated the energy of the odd nuclei when the last odd neutron is in each of the single-particle levels that have been included in the pairing calculations. In the present work, the equations have been solved using a grid size of 0.08 fm. We have assumed that beyond 20 fm, the effect of nuclear interaction vanishes. We have verified that our results are unaffected if a larger distance is taken. For example, an increase to 22 fm changes the total energy by less than 0.005% and radius by less than 0.05% in ^{64}Ca. This convergence is achieved independently of whether we include the width of the positive levels in our calculation or treat it as a zero width level.

The force NLSH [23] has been used in the present work. We have compared our results with a recent relativistic continuum Hartree-Bogoliubov (RCHB) calculation by Zhang et al. [11] who have essentially used a density- and spin-dependent delta-force interaction, strength of which has been fixed by equating the results with Gogny interaction for a particular nucleus. They have included all positive energy states up to the energy cut off value of 120 MeV.

The pairing interaction has been taken to be a delta interaction with a constant

strength, i.e. $V = V_0\delta(\boldsymbol{r_1} - \boldsymbol{r_2})$. The matrix elements are calculated using the wave functions obtained for the single particle states. We have chosen $V_0 = -350$ MeV for the strength of the delta interaction. This value of the strength has been used by Yadav et al. [13]. In the rest of the paper, we will refer to the RMF-BCS calculation with wide resonant states as RMFW, calculation neglecting the width as RMF0, and the results of the RCHB calculation of Ref. [11] as RCHB. We have also calculated the results in the box normalization approach using a box of dimension 20 fm. The results are referred to as BOX.

In Ca isotopes, ^{40}Ca is taken as the core and the pairing window is so chosen that all bound and resonant states above N=20 and below N=82 have been included in the rBCS calculation. For Ni isotopes, ^{56}Ni is the core and all bound as well as resonant states above N=28 and below N=126 have been included. We first discuss our results for the even-even isotopes.

2.1. Even isotopes

In Table 1, we present our results for the binding energy for Ca isotopes and compare with RCHB calculation and also with experimental values wherever available. Here and later, the experimental binding energy values are from Ref. [24].

TABLE 1. Binding energy in MeV *for even* Ca *isotopes in RMFW, RCHB, RMF0, and BOX approaches compared with experimental values. The RCHB results are from Ref. [11]. See the text for details.*

A	RMFW	RCHB	RMF0	BOX	Expt [24]
40	340.96	340.01	340.96	340.96	342.05
42	361.17	360.99	362.18	361.19	361.89
44	380.46	380.09	381.62	380.46	380.96
46	398.75	397.94	398.60	398.75	398.77
48	416.10	414.91	416.10	416.10	415.99
50	425.18	424.44	425.52	425.18	427.49
52	433.79	433.22	434.29	433.80	436.59
54	441.83	441.35	442.50	441.86	444.10[1]
56	449.62	449.00	450.29	449.67	449.79[1]
58	457.24	456.30	457.70	457.28	
60	464.68	463.26	464.68	464.68	
62	465.96	465.32	466.24	466.01	
64	466.88	466.56	467.25	466.99	
66	467.56	467.32	467.51	467.69	
68	468.01	467.75	468.31	468.12	
70	468.30	467.96	468.51	468.40	
72	468.35	467.99	468.61	468.50	
74	468.04	467.64	468.55	468.39	

[1] Estimated value

The values obtained in different procedures are quite close to each other. For Ni isotopes, the corresponding results are given in Table 2. In Fig. 1, we plot the two-

TABLE 2. Binding energy in MeV *for even* Ni *isotopes in RMFW, RCHB, and RMF0 approaches compared with experimental values. The RCHB results are from Ref. [11]. See the text for details.*

A	RMFW	RCHB	RMF0	BOX	Expt [24]
56	484.95	483.50	484.95	484.95	483.99
58	504.23	503.24	504.26	504.22	506.46
60	523.09	522.15	523.12	523.06	523.46
62	541.42	540.34	541.47	541.42	545.26
64	559.14	557.80	559.17	559.09	561.76
66	575.91	574.37	575.94	575.88	576.28
68	591.20	589.51	591.21	591.20	590.41
70	603.66	602.09	603.74	603.57	602.21
72	615.14	613.41	615.32	615.00	613.35
74	625.91	623.98	626.00	625.77	623.75
76	636.06	634.01	636.13	635.95	633.16
78	645.60	643.61	645.60	645.60	641.94
80	647.89	646.36	647.96	647.78	
82	650.31	648.98	650.41	650.09	
84	652.74	651.49	652.89	652.50	
86	655.20	653.85	655.27	654.92	
88	657.39	656.04	656.98	656.95	
90	659.42	658.03	659.61	658.95	
92	661.35	659.85	661.57	661.07	
94	663.27	661.57	663.47	662.94	
96	665.17	663.22	663.32	664.93	
98	667.07	664.78	667.07	667.07	
100	663.99		664.04	663.93	

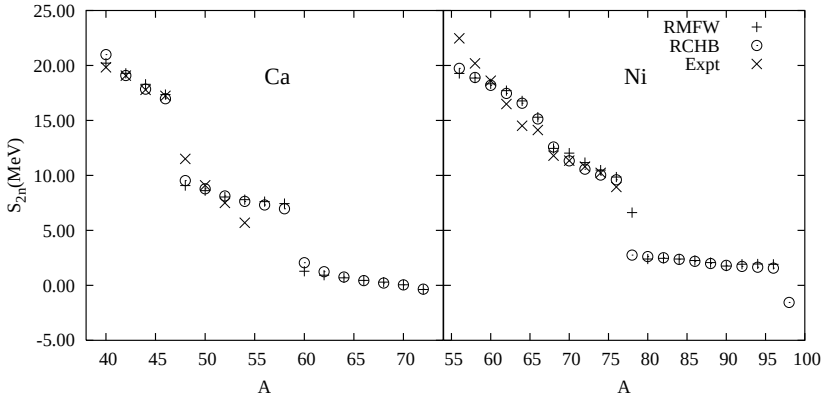

Fig. 1. Two-neutron separation energy in even Ca *and* Ni *isotopes.*

neutron separation energies (S_{2n}) obtained in RMFW and RCHB procedures and compare with experimentally observed values for both elements. As can be seen from Tables 1 and 2, the results for RMFW, RMF0, and BOX are very close to each other. Hence we omit the results for the last two approaches in Fig. 1. We see that the present calculated values compare favourably with the more elaborate and time-consuming RCHB approach. One can see that the experimental trend has been reproduced well. In Ni isotopes, we find that most of our results agree with the constant pairing strength calculation of Cao and Ma [5].

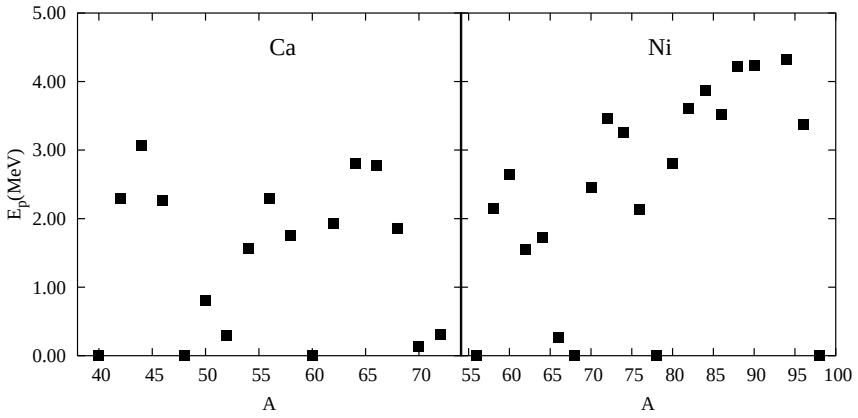

Fig. 2. Pairing energy in RMFW calculation in even Ca *and* Ni *isotopes.*

A very important quantity is the pairing energy defined in the present calculation as E_p = BE(RMF+BCS) – BE(RMF). This is important for the study of the effect of closed shells. We plot our results in Fig. 2. We see that in Ca isotopes, $N = 20$ and $N = 40$ are the magic numbers. For Ni isotopes magicity appears at $N = 40,\ 50$, and more importantly, at $N = 70$. A particularly interesting observation is that $N = 50$ is no longer a magic number for Ca.

The calculated set of magic numbers can be explained on the basis of the single-particle structures in neutron-rich isotopes. The single-particle levels calculated by the RMFW method in these nuclei are shown in Fig. 3. In the neutron-rich Ca isotopes, the $2d_{3/2}$, $2d_{5/2}$ and $3s_{1/2}$ levels come down in energy and approach the $1g_{9/2}$ level. This effect has also been seen in neutron-rich nuclei in other mass regions. The single particle levels in such nuclei often differ significantly from nuclei near the stability valley. In this particular instance, the dramatic relocation of the $3s_{1/2}$ state from the usual position at the top of the *sdg* shell near the stability valley to nearly the bottom of the shell is worth noting. The Fermi level, indicated by the solid line, rises very slowly near the drip line and finally becomes positive for ^{74}Ca. The states $1g_{7/2}$, $1h_{11/2}$, $2d_{3/2}$ and $2d_{5/2}$ remain resonant states in all nuclei. The state $1g_{9/2}$ starts at a positive energy state but, as the neutron number increases, becomes loosely bound. Because of the absence of the centrifugal barrier, the level $3s_{1/2}$ does not have a resonant solution. As already stated, the $3s_{1/2}$ level lies very close to the $1g_{9/2}$ levels in $^{66-72}$Ca.

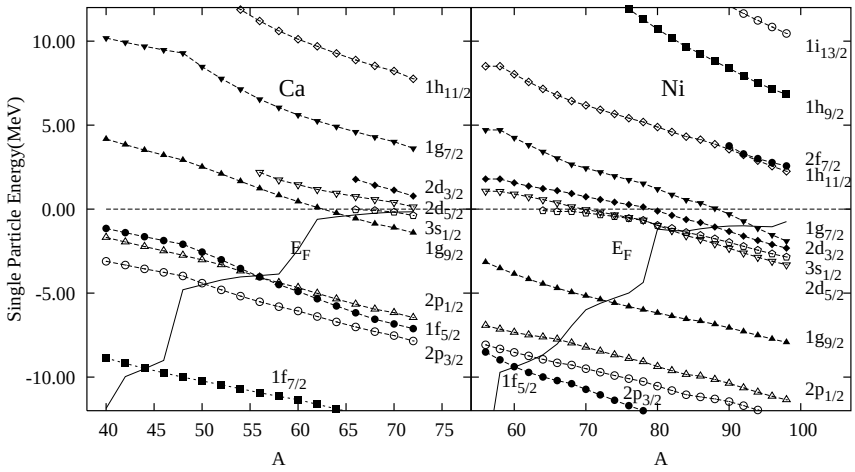

Fig. 3. Single particle neutron energy in the RMFW calculations in even Ca *and* Ni *isotopes. The Fermi level is shown by the continuous line.*

The disappearance of the magic gap at $N = 50$ in Ca nuclei is worth noting. The occupation probability v^2 and the pairing gap Δ values for the different states near the Fermi level in ^{70}Ca are shown in Fig. 4. One can see that the large gap at $N = 40$ is persisting. However, among the states above the Fermi level, the occupancy of the $3s_{1/2}$ state is substantially large. We conclude that there is no shell closure at $N = 50$. The disappearance of the shell closure at $N = 50$ in neutron-rich isotopes has earlier been observed in many theoretical studies. In a study of neutron-rich Cr and Fe isotopes [25], we also have seen the same effect. However, in Fig. 2 one can still see a substantial drop in the pairing energy at $N = 50$, indicating the closure of the $1g_{9/2}$ subshell. Such a drop is also observed at

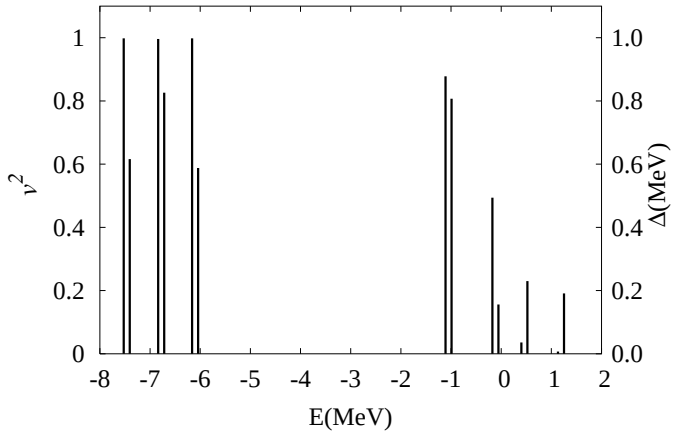

Fig. 4. Occupation factors and pairing gap for single neutron states in ^{70}Ca *plotted against the energy of the state. The left (right) axis and columns represents occupation factor (pairing gap) for different levels around the Fermi surface.*

$N = 32$, corresponding to the closure of $2p_{3/2}$ subshell. The calculated occupancy factors for the levels in the *sdg* shell in nuclei with $A > 60$ are give in Table 3. One can see that for $N = 52$, the occupancy of the $2d_{5/2}$ state is appreciable. This is the reason that, contrary to Ref. [13], the pairing energy actually increases from ^{70}Ca to ^{72}Ca in our calculation. The states $1g_{9/2}$, $3s_{1/2}$ and $2d_{5/2}$ lie very close to each other in neutron-rich Ca nuclei, thus no shell closure beyond $N = 40$ is observed in Ca nuclei within the neutron drip line.

TABLE 3. The calculated occupancy (v^2) values in $^{62-72}$Ca isotopes for the states in the sdg shell. Also shown are the number of nucleons in the continuum (N_h).

	States					
A	$1g_{9/2}$	$1g_{7/2}$	$2d_{5/2}$	$2d_{3/2}$	$3s_{1/2}$	N_h
62	0.207	0.002	0.004			2.110
64	0.405	0.002	0.008			0.064
66	0.592	0.003	0.013	0.004	0.026	0.118
68	0.764	0.003	0.022	0.006	0.120	0.180
70	0.878	0.003	0.036	0.007	0.495	0.268
72	0.949	0.003	0.114	0.008	0.895	0.740

In even Ni isotopes, the Fermi level is deeper and abruptly becomes positive beyond $A = 98$. The levels $3s_{1/2}$, $1g_{7/2}$, $2d_{3/2}$ and $2d_{5/2}$ lie very close to each other. All of them, except the first, start as positive energy states and become bound states at higher neutron number. The intruder orbit $1h_{11/2}$ lies much higher in energy. This is a consequence of the quenching of the spin-orbit splitting in neutron-rich nuclei which has been obtained in many mean-field calculations and also experimentally observed in light nuclei. Thus $N = 70$ becomes a new magic number.

It is interesting to compare the results for ^{60}Ca from the present calculation with that of analytic continuation method [17]. For example, with the same NLSH force, they have obtained the energy of the $1g_{9/2}$ state as 0.47 MeV and the width of the state as 0.0004 MeV. The corresponding values in our calculation are 0.45 MeV and 0.0014 MeV, respectively.

In Figs. 5 and 6, we have plotted the large components of the wave functions of the resonant states in ^{60}Ca and ^{70}Ca, respectively. One can see that these states are indeed localized. The function corresponding to the $1g_{9/2}$ state in ^{60}Ca can be compared to the one obtained by Zhang et al. in [17]. One can see that they are very similar. It should be noted that in some nuclei, some of the states could not be localized as the centrifugal barrier was not sufficient for this purpose. For example, in Ca nuclei, although the $1g_{7/2}$ and $1h_{11/2}$ states, because of their high angular momenta, are localized in all studied nuclei, localized solutions for $2d_{3/2}$ were obtained only for $A \geq 66$ and, for $2d_{5/2}$ only for $A \geq 56$. Because of the absence of the centrifugal barrier, no resonant solution for $3s_{1/2}$ was obtained and bound state solutions were obtained for $A \geq 66$.

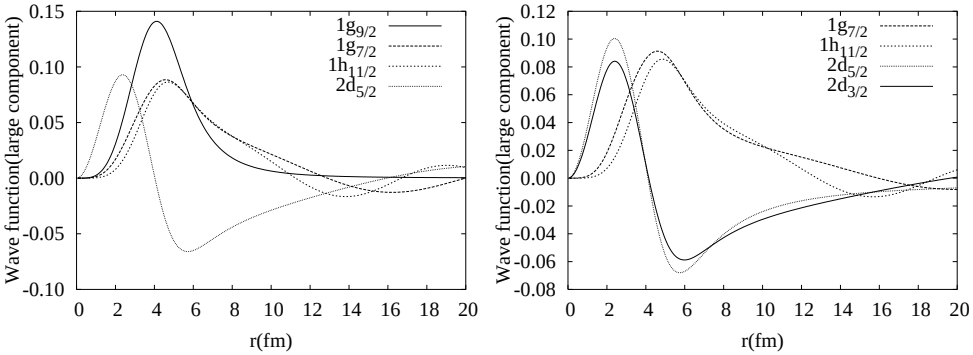

Fig. 5 (left). Large component of the wave functions of resonant continuum states in ^{60}Ca *in the RMFW approach. The states are indicated in the figure.*

Fig. 6. Large component of the wave functions of the resonant continuum states in ^{70}Ca *in the RMFW approach. The states are indicated in the figure.*

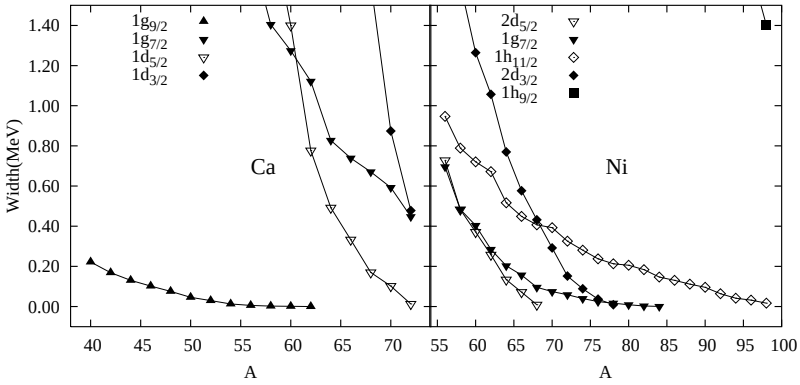

Fig. 7. Widths of the continuum states as a function of mass number in even Ca *and* Ni *isotopes.*

In Fig. 7, we have shown the width of some resonant states as functions of the mass number. In Ca nuclei, the $1g_{9/2}$ states are very narrow and can actually be treated as quasi-bound states. As the neutron number increases, the energy values of the resonant states decrease. Simultaneously, they become narrower. This trend is observed in Fig. 8 where we plot the results for Ca isotopes only. Thus a wide state first becomes narrow and ultimately may become a loosely-bound state. The trend is similar in Ni (not shown).

Another interesting feature is observed for the neutron radii (r_n). The different calculated values are shown in Fig. 9. We have already mentioned that the effect of increasing the cut-off distance of the integrals on the neutron radii is very small. From the figure it is seen that the values from different calculations for Ca agree very well except in $A = 70, 72$ where the RMF values are larger than the RHB results.

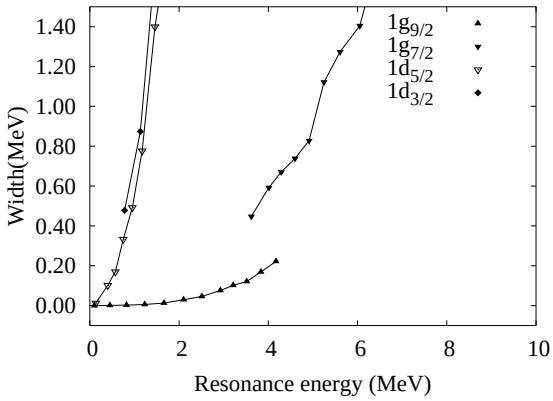

Fig. 8. Widths of the continuum states as a function of resonance energy in even Ca *isotopes.*

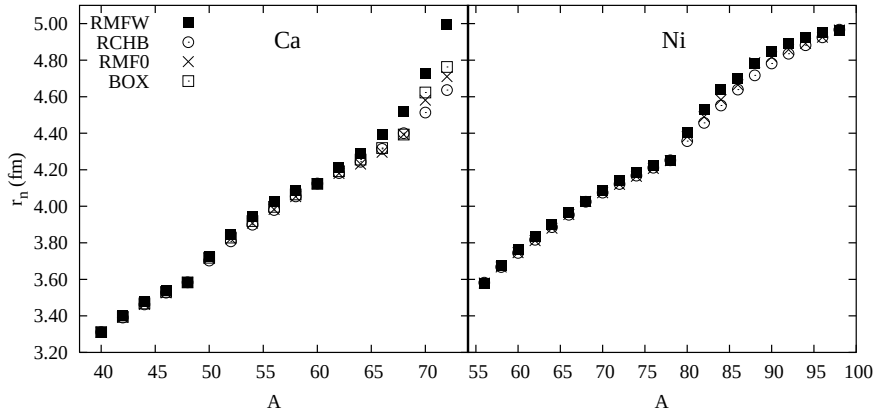

Fig. 9. Neutron radii in different calculations in even Ca *and* Ni *isotopes.*

Sandulescu et al. [4] have pointed out that this difference is generally common near the drip line and can be attributed to the different methods of pairing calculation. The occupancies of narrow resonances with high angular momenta are higher in RHB calculation. This is a consequence of the large energy cut off employed in the RHB (or HFB) approach which makes the Fermi sea more diffuse, thus increasing the scattering to loosely bound states and the narrow resonances with high angular momenta. The RMF calculations, on the other hand, predict increased occupancy of broader low angular momentum resonances. The radius near the drip line depends very sensitively on the occupancy of the localized orbits. The high spin states are more localized due to the larger centrifugal barrier. Increased occupancy for them translates into smaller radius for RHB calculation. Interestingly, one can see that neglecting the width of the single-particle levels actually tends to make the radii values close to the RHB results. The occupation probabilities of the neutron single-particle states near the Fermi level in ^{72}Ca are shown in Table 4. One can

TABLE 4. Comparison of single particle energy values in MeV *and occupation probabilities of the drip line nucleus* ^{72}Ca *in different procedures.*

	RMFW		RMF0		BOX	
State	Energy	v^2	Energy	v^2	Energy	v^2
$1g_{9/2}$	-1.405	0.949	-1.243	0.967	-1.274	0.998
$1g_{7/2}$	3.620	0.003	3.886	0.001	4.246	0.002
$2d_{5/2}$	0.124	0.114	0.334	0.066	0.344	0.099
$2d_{3/2}$	0.779	0.008	1.034	0.004	0.963	0.007
$3s_{1/2}$	-0.376	0.895	-0.217	0.958	-0.255	0.953

see that the occupancies of the broad resonant state $2d_{5/2}$ decrease and that of the high-spin $1g_{9/2}$ state increases if one neglects the width. The results of box normalization lies in-between the RMFW and RMF0 results. In our calculation, the $3s_{1/2}$ level becomes bound in ^{66}Ca. The wave function of this state extends to a large distance outside the nucleus because of the absence of the centrifugal barrier. Thus the neutron radius tends to increase faster beyond ^{64}Ca as the occupancy of the $3s_{1/2}$ level becomes appreciable. In ^{70,72}Ca, the occupancy of the $3s_{1/2}$ level is large. The large components of the wave functions of the bound neutron states in ^{72}Ca above $N = 20$ are shown in Fig. 10. One can see that the $3s_{1/2}$ state has a large tail outside the nucleus because of the absence of the centrifugal barrier for this state. Thus the two nuclei ^{70,72}Ca show a sudden increase in the tail part of the density.

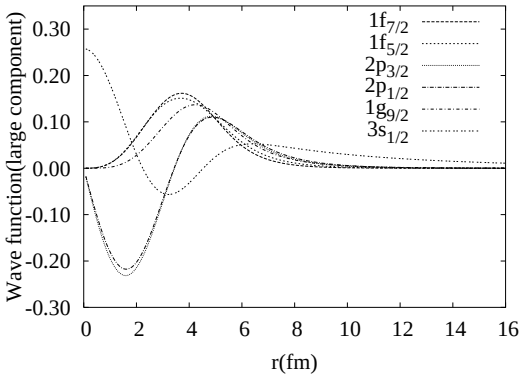

Fig. 10. Large components of the wave functions of the bound neutron states in ^{72}Ca *in the RMFW approach.*

The fact that the drip line in Ni occurs at a magic number implies that the radius tends to saturate there. The neutron radius plotted in Fig. 9 exhibits this feature. The neutron radius saturates at $N = 70$, the new magic number, a property shared by all other calculations. The results of BOX calculation are very close to RMF0 and are not shown for Ni isotopes. One interesting feature in Ni is that the shell closure at $N = 40$ is less pronounced than those at $N = 50$ or $N = 70$, as

evident from the trend. Thus, due to the magicity of $N = 70$, no halo is observed in Ni isotopes.

It is clear from Fig. 9 that the RMF0 predicts a smaller radius compared to RMF. To explicitly show the effect of the width of the resonant states on the density and the radius, we plot the neutron density obtained in RMFW and RMF0 calculation for ^{70}Ca in Fig. 11. It is well known that that ignoring the width of the resonant levels makes the pairing energy higher. This indicates more binding and consequently less diffuseness of the neutron tail and a smaller neutron radius in RMF0 approach compared to RMFW.

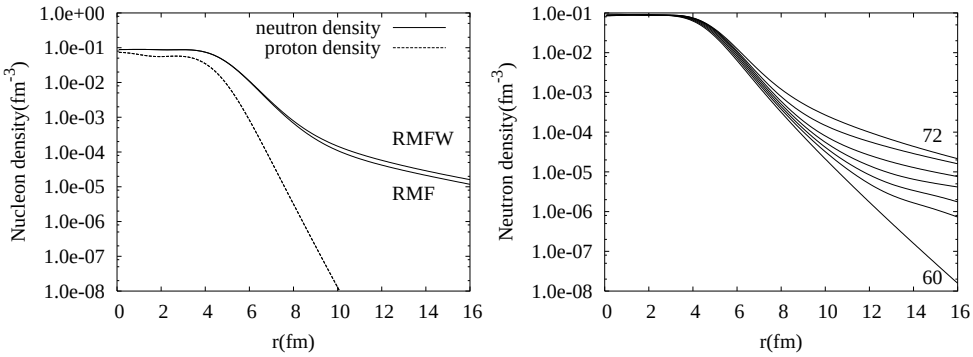

Fig. 11 (left). Comparison of neutron density in ^{70}Ca *in the RMFW and RMF0 approaches.*

Fig. 12. Neutron density in some of the Ca *nuclei with* $A \geq 60$ *in the RMFW approach. The mass numbers of the isotopes are indicated in the figure.*

In Fig. 12 we plot the neutron densities obtained from RMFW calculation for some of the neutron rich Ca isotopes. One can clearly see the sudden increase in ^{62}Ca showing a halo-like behaviour. To explicitly illustrate the halo effect in neutron rich nuclei, we refer to the occupancy of the different levels in *sdg* shell in $^{62-72}$Ca shown in Table 3. The number of neutrons in the resonant states (N_h), i.e., the number of halo nucleons, are shown in the last column. One can see that the most pronounced halo is observed in ^{62}Ca. This is due to the $1g_{9/2}$ state being a just unbound resonant state in ^{62}Ca. The number of halo nucleons in ^{62}Ca agrees with that obtained in the RCHB calculation. However, for heavier nuclei, the RCHB results predict a higher number of halo neutrons. For example, the corresponding numbers in ^{70,72}Ca are 1.9 and 2.7, respectively. As shown in Fig. 10, the $3s_{1/2}$ level is very weakly bound and its wave function extends to a large distance. Thus the number of neutrons outside the compact radius is actually larger than indicated by N_h.

Comparison of the halo with other calculations in neutron-rich exotic nuclei may be interesting. The possibility of a giant halo in very neutron-rich Zr nuclei with up to six neutrons in the halo were predicted in Ref. [26]. Possibilities of giant halo in Ca nuclei has already been explored in RCHB approach [11, 12]. Terasaki et al.

[27] investigated neutron-rich Ca nuclei in RCHB and Skyrme HFB approaches for possible sign of giant halos. Grasso et al. [16] also investigated Ca nuclei using the latter approach. It is seen that the halo sensitively depends on the method followed. Even different Skyrme forces in the non-relativistic calculations do not yield the same results. We have already pointed out that RCHB calculations predict a larger halo than our calculation. For example, the occupancy of the $3s_{1/2}$ state in RCHB calculation [27] using the same NLSH force is 0.089 while we find a value of 0.026. In fact our value is much closer to the nonrelativistic results.

2.2. Odd isotopes

We have calculated the binding energy corresponding to the different single-particle levels in odd nuclei in the blocked BCS approximation. Although the ground state spin parity is unknown in many of the nuclei, we find that, except for ^{75}Ni, the spin parity has been correctly predicted wherever the ground state is unambiguously known. We have already reported some of our results for neutron-rich nuclei in Ref. [18]. We have come across no RHB calculation for odd mass Ca or Ni isotopes.

We present the results for binding energy and radius in odd Ca and Ni nuclei in Tables 5 and 6. Only the RMFW results are tabulated as the results for RMF0 and BOX calculations are very similar.

TABLE 5. Binding energy and neutron radius for odd Ca *isotopes in RMFW approach compared with experimental values.*

	B.E.(MeV)		r_n(fm)		B.E.(MeV)		r_n(fm)
A	RMFW	Expt[24]	RMFW	A	RMFW	Expt[24]	RMFW
41	349.84	350.41	3.352	51	428.85	431.85	3.779
43	369.60	369.83	3.435	53	436.86	440.01	3.900
45	388.40	388.37	3.509	55	444.92	446.38	4.026
47	406.23	406.04	3.555	57	452.65	451.55	4.040
49	420.13	421.14	3.638	59	460.15		4.098
61	464.26						

As pointed out in Ref. [18], the striking features for these two chains of isotopes are the differences in the position of the drip line for odd and even isotopes. In Ca isotopes, the last odd-mass nucleus stable against neutron emission is ^{59}Ca while the corresponding even mass isotope is ^{72}Ca. On the other hand, the corresponding drip line nuclei in Ni are ^{97}Ni and ^{98}Ni, respectively. In other words, all Ni isotopes are stable against neutron emission up to $N = 70$ beyond which neither the even nor the odd isotopes are stable for this element. For Ca, the odd isotopes are stable below $N = 40$ while stable even isotopes range up to $N = 52$.

TABLE 6. Binding energy and neutron radius for odd Ni *isotopes in RMFW approach compared with experimental values.*

	B.E.(MeV)		r_n(fm)		B.E.(MeV)	r_n(fm)
A	RMFW	Expt[24]	RMFW	A	RMFW	RMFW
57	495.53	494.24	3.624	79	646.30	4.250
59	512.57	515.46	3.711	81	648.70	4.406
61	531.08	534.56	3.791	83	651.15	4.533
63	549.30	552.10	3.857	85	653.55	4.642
65	566.58	567.86	3.921	87	655.80	4.717
67	583.34	582.61	3.990	89	657.87	4.784
69	596.16	594.99	4.029	91	659.62	4.850
71	608.18	606.34	4.090	93	661.43	4.894
73	619.35	617.14	4.141	95	663.37	4.927
75	629.83	627.37	4.186	97	665.28	4.952
77	639.68	636.33	4.223	99	665.03	

The reason for this difference has been traced to the new magic numbers in neutron-rich nuclei. As already pointed out, in Ca isotopes, the last neutron magic number is $N = 40$ and the magic gap at $N = 50$ vanishes. The single-particle levels beyond $N = 40$ are either in the continuum or very loosely bound. Importantly, in Ca isotopes, the level $1g_{9/2}$ lies either in the continuum or just bound around $N = 40$. Hence the stability of the isotopes depends crucially on the pairing interaction and the contribution of the states in the continuum. Thus the odd-mass Ca isotopes beyond $N = 40$ are unstable against neutron emission. On the other hand, the Ni isotopes present a completely different picture. Here, $N = 70$ is a new magic number and the levels below it are bound by more than 2 MeV. Because of the comparatively larger binding energy, the binding energy of the odd nuclei does not depend overmuch on the pairing. Hence we obtain both even and odd mass nuclei which are stable against particle emission up to the new magic number $N = 70$.

3. Summary

We have studied the effect of the resonant continuum on drip line in Ca and Ni nuclei. We find that only a few positive energy resonant states along with the bound states are sufficient to produce results comparable to the RCHB approach for the total quantities like binding energy, radius, two-neutron separation energy, etc. in most cases. The nuclei ^{70,72}Ca show a sudden increase in the tail of the density distribution. This can be traced to the fact that in these nuclei, the occupancy of the $3s_{1/2}$ state is substantially large. This state being very weakly bound and having no centrifugal barrier extends outside the nucleus radius to a large distance creating a neutron halo. In Ca isotopes, the magic number at $N = 50$ vanishes while in Ni isotopes, a new magic number appears at $N = 70$. Ni isotopes do not show any

neutron halo. The new sequence of magic numbers leads to an interesting difference in the drip line for the even and odd isotopes in the two chains. In the Ca isotopes, the last bound even and odd nuclei are found to be ^{72}Ca and ^{59}Ca, respectively. In Ni isotopes, the corresponding nuclei are ^{98}Ni and ^{97}Ni, respectively. The resonance states and the very shallow bound states play an important role in the formation of the neutron halo in Ca isotopes. We should mention here that all specific results for the drip line, occupancy of single particle states, etc. are for the NLSH force and may vary for other forces, a situation encountered in nonrelativistic calculations [16].

Acknowledgements

This work was carried out with financial assistance of the Board of Research in Nuclear Sciences, Department of Atomic Energy (Sanction No. 2005/37/7/ BRNS).

References

[1] See *e.g.* B. Jonson, Phys. Rep. **389** (2004) 1 and references therein.

[2] M. Grasso, N. Sandulescu, N. Van Giai and R.J. Liotta, Phys. Rev. C **64** (2001) 064321.

[3] M. Grasso, N. Van Giai and N. Sandulescu, Phys. Lett. **B535** (2002) 103.

[4] N. Sandulescu, L.S. Geng, H. Toki and G.C. Hillhouse, Phys. Rev. C**68** (2003) 054323.

[5] L. Cao and Z.Y. Ma, Eur. Phys. J. A **22** (2004) 189.

[6] S.A. Fayans, S.V. Tolokonnikov and D. Zawischa, Phys. Lett. **B491** (2000) 245.

[7] S. Im and J. Meng, Phys. Rev. C **61** (2000) 047302.

[8] B.Q. Chen, Z.Y. Ma, F. Grummer and S. Krewald, Phys. Lett. **B455** (1999) 13.

[9] J. Meng and P. Ring, Phys. Rev. Lett. **77** (1996) 3963; J. Meng, Nucl. Phys. **A635** (1998) 3.

[10] J. Meng, H. Toki, J.Y. Zeng, S.Q. Zhang and S.-G. Zhou, Phys. Rev. C**65** (2002) 041302.

[11] S.Q. Zhang, J. Meng, H. Toki, I. Tanihata and S.-G. Zhou, Science in China **G46** (2003) 632.

[12] J. Meng, H. Toki, S.-G. Zhou, S.Q. Zhang, W.H. Long and L.S. Geng, Prog. Part. Nucl. Phys. **57** (2006) 470.

[13] H.L. Yadav, M. Kaushik and H. Toki, Int. Jour. Mod. Phys. E **13** (2004) 647.

[14] S.-G. Zhou, J. Meng and P. Ring, Phys. Rev. C **68** (2003) 034323.

[15] J.Terasaki, P.-H. Heenen, H. Flocard and P. Bonche, Nucl. Phys. **A600** (1996) 371.

[16] M. Grasso, S. Yoshida, N. Sandulescu and N. Van Giai, Phys. Rev. C **74** (2006) 064317.

[17] S.S. Zhang, J. Meng, S.G. Zhou and G.C. Hillhouse, Phys. Rev. C**70** (2004) 034308.

[18] M. Bhattacharya and G. Gangopadhyay, Phys. Rev. C **72** (2005) 044318.

[19] See *e.g.* B.D. Serot and J.D. Walecka, Adv Nucl. Phys., **16** (1986) 1; Y.K. Gambhir, P. Ring and A. Thimet, Ann. Phys. (N.Y.), **198** (1990) 132; P. Ring, Prog. Part. Nucl. Phys. **37** (1996) 13.

[20] See *e.g.* J. Horowitz and B.D. Serot, Nucl. Phys. **A368** (1981) 503.

[21] J. Boguta and A.R. Bodmer, Nucl. Phys. **A 292** (1977) 414.

[22] A.B. Migdal, A.M. Perelemov and V.S. Popov, Sov. J. Nucl. Phys. **14** (1971) 488.

[23] M.M. Sharma, M.A. Nagarajan and P. Ring, Phys. Lett. **B312** (1993) 377.

[24] G. Audi, A.H. Wapstra and C. Thibault, Nucl. Phys. **A729** (2003) 337.

[25] P. Mitra and G. Gangopadhyay, Int. Jour. Mod. Phys. E **13** (2004) 1209.

[26] J. Meng and P. Ring, Phys. Rev. Lett. **80** (1998) 460.

[27] J. Terasaki, S.Q. Zhang, S.G. Zhou and J. Meng, Phys. Rev. C **74** (2006) 054318.

STANJA KONTINUUMA U JEZGRAMA KALCIJA I NIKLA BOGATIM NEUTRONIMA

Istražujemo učinak rezonantnog kontinuuma u jezgrama Ca i Ni blizu granice bijega. Riješili smo relativističke jednadžbe za srednje polje primjenom uvjeta za raspršenje za stanja pozitivne energije. Sparivanje se uvodi međudjelovanjem nultog dosega a BCS jednadžbe smo riješili uključujući rezonantna stanja. Naši računi mogu u većini slučajeva dati vrijednosti za energiju vezanja, polumjer, dvoneutronsku energiju odvajanja, itd. Jezgre ^{70,72}Ca pokazuju nagao porast repa raspodjele gustoće kako se, zbog slabog vezanja i izostanka centrifugalne barijere, stanje $3s_{1/2}$ proširuje daleko izvan polumjera jezgre, stvarajući neutronski halo. Izotopi nikla ne pokazuju neutronski halo. Pojava magičnih brojeva i nestanak ranijih u izotopima bogatim neutronima vodi do dramatičnih promjena linije bijega u parnim i neparnim jezgrama oba niza.